electronic reprint

Journal of
Applied Crystallography
ISSN 0021-8898
Editor: **Gernot Kostorz**

Reliability criteria in quantitative texture analysis with experimental and simulated orientation distributions

Daniel Chateigner

Journal of
Applied Crystallography
ISSN 0021-8898

Received 17 March 2004
Accepted 28 April 2005

Reliability criteria in quantitative texture analysis with experimental and simulated orientation distributions

Daniel Chateigner

Laboratoire CRISMAT, ENSICAEN, UMR CNRS 6508, 6 Bd. M. Juin, Caen, France. Correspondence e-mail: daniel.chateigner@ensicaen.fr

Quantitative texture analysis reliability factors are examined from an experimental point of view, using real-sample and modelled orientation distribution refinements. The classical *RP* factors of texture analysis are shown to depend on the texture strength, and their representation of the various textures is not homogeneous. The surface-weighted RP_w homologues exhibit lower texture strength dependency and better homogeneities, but still do not allow for comparison of refinements operated on samples with different textures. New factors, R_w, weighted by the counting statistics, show the lowest dependency and best homogeneity. From $R_{w1}(R_{w0})$ curves a new criterion is established, which allows the detection of poorly refined orientation distributions. This study highlights a unique entropy-to-texture index relationship, which also gives a new criterion for testing refinement reliability, and proposes two different ranges in which to apply the texture index and the entropy factors.

1. Introduction

The reliability of refined structures has given rise to long debates in the crystallography literature since the earliest data fits. Finding reliable and comparable estimators to test different structural solutions is not a simple task, and normalized means and standard deviations remain the most used parameters for the measurement of statistical agreements between observed and simulated data (Young *et al.*, 1982). Very rare use is made in the literature of more sophisticated descriptors, such as the generalized weighted *R* factors and *R*-factor ratio (Hamilton, 1965), or the 'jackknife'-derived approach (Rothstein *et al.*, 1978), which are aimed at helping crystallographers to decide whether a larger number of fitted parameters lead to a significant improvement of the fit. Furthermore, *R* factors have been proved experimentally to depend on the number of independent parameters of the refinements, on whether experimental backgrounds are taken into account or not in the observations (Hill & Fisher, 1990), and finally on program implementations, giving rise to apparently equivalent *R*-factor definitions for practically very different estimators.

In quantitative texture analysis (QTA), as a general trend, the case is even worse, and there is no systematic use of reliability factors to account for the reliability of the orientation distribution function (ODF) refinement, although *R* factors have been formally introduced for more than 15 years (Matthies *et al.*, 1987). This oversight is mainly due to the relatively late development of iterative processes of ODF refinements, using generalized spherical harmonics (Bunge & Esling, 1982), vector (Ruer & Baro, 1977), WIMV (Williams–Imhof–Matthies–Vinel; Matthies & Vinel, 1982), ADC (arbitrarily defined cells) (Pawlik, 1993) or entropy maximization (Toraya, 1986) approaches. However, the necessary introduction of reliability estimators is also a more complex task than in whole-powder-pattern or Rietveld (1969) fitting, for two main reasons. Firstly, the values to be refined are orientation densities, quantities defined in the $[0, \infty]$ real numbers interval, which are normalized to a perfectly randomly oriented powder from the diffracted intensities. Consequently, the orientation distribution space is non-linearly deformed, defective density levels being represented in the [0, 1] interval, whereas orientation reinforcements are in the range $[1, \infty]$, the 1 m.r.d. (multiple of the random distribution) value being associated with the peculiar reference of the random powder. Secondly, using diffraction experiments, the orientation distribution space is always underdetermined. In this work we introduce new reliability descriptors in texture analysis. Their relevance is compared with that of previously described indicators in terms of variability with texture strength, using the texture index and entropy values as overall quantities to represent levels of densities. We compare two series of refined ODFs: one from approximately 150 real samples and the other from synthetic standard data.

2. QTA-related observations

QTA relies on the measurement of pole figures, which are used for the ODF refinement (Kocks *et al.*, 1998). For a perfectly randomly oriented powder (sample without texture), the intensity diffracted by the $\{hkl\}$ planes is constant whatever the sample orientation $\mathbf{y} = (\vartheta, \varphi)$ (ϑ and φ being two

Euler angles locating the $\mathbf{h} = \langle hk\ell \rangle^*$ directions in a chosen reference frame). In the case of a textured sample, this intensity, $I_{\mathbf{h}}(\mathbf{y})$, varies in a different fashion for each $\mathbf{h}$ pole figure, and a typical quantitative measurement of the texture requires several hundreds of $\mathbf{y}$ sample orientations for each $\mathbf{h}$. However, the ODF remains underdetermined. For instance, considering a triclinic crystal system and a 5°-resolution grid of the ODF, and if 50 complete pole figures can be measured, 68400 observations are measured in total, whereas the ODF requires the determination of 98496 densities. Increasing the crystal symmetry ameliorates the ODF determination completeness by a decrease in symmetry-independent densities to be determined. In addition, the number of pole figures and sample orientations to measure depends on many parameters, such as crystal symmetry, experimental setup or resolution of the desired ODF (Bunge, 1982; Wenk, 1985; Matthies & Vinel, 1982). All this gives rise to complex determinations of usually described reliability parameters such as R_{expected} (Hill & Fisher, 1990), for which the number of independent observations, parameters and constraints are required, and may explain why little use is made of these methods in texture analysis.

Since the only concern of texture analysis is the orientation of crystallites, all effects such as porosity, crystalline and stress states, thicknesses, absorption, and phase contents, which are present in the diffracted intensities, have to be removed. This end is achieved through a normalization procedure, part of the ODF refinement, resulting in the experimental normalized pole figures $P_{\mathbf{h}}(\mathbf{y})$. Once the ODF has been refined, any normalized pole figure can be recalculated: for instance, the initially measured ones for comparison. The diffracted intensities $I_{\mathbf{h}}(\mathbf{y})$ are integrated intensities corrected for any diffracted background, and so then are the distribution densities $P_{\mathbf{h}}(\mathbf{y})$. The link between $I_{\mathbf{h}}(\mathbf{y})$ and $P_{\mathbf{h}}(\mathbf{y})$ is a normalization factor $N_{\mathbf{h}}$ defined by $I_{\mathbf{h}}(\mathbf{y}) = P_{\mathbf{h}}(\mathbf{y})N_{\mathbf{h}}$.

Many different formalisms may be used for ODF refinements, each of them presenting its own advantages (Wenk *et al.*, 1994). In this study, the WIMV approach has been utilized, mainly because all the data were allowable after about ten years of intensive use of this formalism. The used data were not intended at the beginning to serve this study, since human-related errors, such as experience in using the methodology, are included in the results. However, no correlation is expected between the refiner's expertise and texture strength, and the sole consequence of using such a sample may be a slightly larger standard deviation of the results than if refinements were carried out over a short period of time.

3. ODF refinement reliability estimators

The calculations need as inputs the experimental and WIMV-recalculated normalized pole figures. We used the WIMV algorithm implemented in the *BEARTEX* program package (Wenk *et al.*, 1998), and estimators were calculated from these data using *Pofint* (Chateigner, 2002).

3.1. *RP* factors

The best solution found for the orientation distribution $f(g)$ is in the WIMV algorithm incorporated in *BEARTEX*. That for the minimum averaged reliability factors is given by

$$\overline{RP}_x = \frac{1}{I}\sum_i\sum_j \frac{|P^{\text{c}}_{\mathbf{h}_i}(\mathbf{y}_j) - |P^{\text{o}}_{\mathbf{h}_i}(\mathbf{y}_j)|}{P^{\text{o}}_{\mathbf{h}_i}(\mathbf{y}_j)}, \qquad (1)$$

where $\mathbf{h}_i$, $i = 1, \ldots, I$, are the measured pole figures and $\mathbf{y}_j$, $j = 1, \ldots, J$, are the measured points of the pole figures. The superscripts o and c denote, respectively, observed-normalized and WIMV-recalculated-normalized pole figures.

The *RP* factors are known to depend on the texture strength, even though this dependency has never been illustrated. Therefore, they are very suitable for the refinement steps itself, this sensitivity somehow helping the program to detect better solutions. This dependency results from the absence of any weighting scheme in their formulation, *i.e.* by the orientation density levels. Consequently, the comparison of refinement quality between samples using *RP* factors remains ambiguous. In other words, one should compare the refinement quality with *RP* factors only for similar texture strengths, texture components and measurement resolutions.

In order to discriminate the reliabilities of different density levels, Matthies *et al.* (1987) introduced the criterion x, which serves as a threshold for the densities entering the calculations. Hence, for one pole figure, the 'individual relative deviation' factor is defined by

$$RP_x(\mathbf{h}_i) = \frac{\sum_{j=1}^{J}\left|P^{\text{o}}_{\mathbf{h}_i}(\mathbf{y}_j) - P^{\text{c}}_{\mathbf{h}_i}(\mathbf{y}_j)\right|}{\sum_{j=1}^{J} P^{\text{o}}_{\mathbf{h}_i}(\mathbf{y}_j)}\,\theta\left[x, P^{\text{o}}_{\mathbf{h}_i}(\mathbf{y}_j)\right], \qquad (2)$$

with

$$\theta\left[x, P^{\text{o}}_{\mathbf{h}_i}(\mathbf{y}_j)\right] = \begin{cases} 1 \text{ for } P^{\text{o}}_{\mathbf{h}_i}(\mathbf{y}_j) > x \\ 0 \text{ for } P^{\text{o}}_{\mathbf{h}_i}(\mathbf{y}_j) \le x, \end{cases}$$

$$x = 0, \epsilon, 1, 10.$$

The value x is a criterion used to appreciate the quality of the refinement for different density levels. Using $x = 1$ reveals only the reliability of the poles above 1 m.r.d., *i.e.* those poles representative of textured area. Since $P^{\text{o}}_{\mathbf{h}_i}(\mathbf{y}_j)$ can be equal to zero, we generally use $x = 0.05$ to reveal the global quality.

These individual factors help to detect if some pole figures are particularly badly reproduced after the refinement, in order to operate to a correction strategy. However, the total reliability of the ODF calculation can be checked using a mean value among all individual pole figures, giving the 'averaged relative deviation factors

$$\overline{RP}_x = \frac{1}{I}\sum_{i=1}^{I} RP_x(\mathbf{h}_i) \qquad (3)$$

or

$$RP_x = \frac{\sum_{i=1}^{I}\sum_{j=1}^{J}\left|P^{\rm o}_{\mathbf{h}_i}(\mathbf{y}_j) - P^{\rm c}_{\mathbf{h}_i}(\mathbf{y}_j)\right|}{\sum_{i=1}^{I}\sum_{j=1}^{J}P_{\mathbf{h}_i}(y_j)}\,\theta\left[x, P^{\rm o}_{\mathbf{h}_i}(\mathbf{y}_j)\right], \qquad (4)$$

which can be used to compare ODF reliabilities between samples, in the hypothesis of similar textures, as will be seen later.

3.2. RP_w surface-weighted factors

Matthies *et al.* (1987) also proposed reliability factors weighted by the surface area of the measured cells $\mathbf{y}$ of the pole figures, in order to account for the solid angle in which the diffracted intensity is distributed. The averaged surface-weighted factors are calculated by

$$\overline{RP}_{wx} = \sum_{i=1}^{I}\frac{\sum_{j=1}^{J}S_j\left|P^{\rm o}_{\mathbf{h}_i}(\mathbf{y}_j) - P^{\rm c}_{\mathbf{h}_i}(\mathbf{y}_j)\right|}{\sum_{j=1}^{J}S_jP^{\rm o}_{\mathbf{h}_i}(\mathbf{y}_j)}\,\theta\left[x, P^{\rm o}_{\mathbf{h}_i}(\mathbf{y}_j)\right] \qquad (5)$$

or

$$\overline{RP}_{wx} = \frac{\sum_{i=1}^{I}\sum_{j=1}^{J}S_j\left|P^{\rm o}_{\mathbf{h}_i}(\mathbf{y}_j) - P^{\rm c}_{\mathbf{h}_i}(\mathbf{y}_j)\right|}{\sum_{i=1}^{I}\sum_{j=1}^{J}S_jP^{\rm o}_{\mathbf{h}_i}(\mathbf{y}_j)}\,\theta\left[x, P^{\rm o}_{\mathbf{h}_i}(\mathbf{y}_j)\right], \qquad (6)$$

where

$$S_j = \Delta\varphi\left[\cos\left(\vartheta_j - \Delta\vartheta/2\right) - \cos\left(\vartheta_j + \Delta\vartheta/2\right)\right],$$
$$S_0 = \pi(1 - \Delta\vartheta/2) \text{ (surface element for } \mathbf{y}_j),$$

in which the individual factors are recognized.

3.3. *RB* Bragg-like factors

Another R factor, corresponding to the Bragg R factor of Rietveld analysis, would be interesting to calculate. We will call this the Bragg-like standard deviation factor. This factor takes the same formulation as the RP factors, which also stands if densities are replaced by intensities, since the normalizing factor simplifies in the expression:

$$RB_x(\mathbf{h}_i) = \frac{\sum_{j=1}^{J}\left|I^{\rm o}_{\mathbf{h}_i}(\mathbf{y}_j) - I^{\rm c}_{\mathbf{h}_i}(\mathbf{y}_j)\right|}{\sum_{j=1}^{J}I^{\rm o}_{\mathbf{h}_i}(\mathbf{y}_j)}\,\theta\left[x, P^{\rm o}_{\mathbf{h}_i}(\mathbf{y}_j)\right]. \qquad (7)$$

$R_{\rm Bragg}$ factors have been introduced in order to compare powder diffraction to single-crystal results. However, for textured samples, the integration has to be extended to all the i and j points. One can notice that their expression in texture analysis is the same as that for RP factors [equation (2)]. However, the intensities entering the calculation are 2θ-integrated peaks, as in Rietveld analysis; then the $RB_x(\mathbf{h}_i)$ factors are meaningless for pole figures measured using point detectors.

3.4. R_w weighted factors

The Rietveld-like or 'intensity-weighted' R factors, which take into account the normal Gaussian distribution standard deviation for each measured intensity, can also be evaluated:

$$R_{wx}(\mathbf{h}_i) = \left\{\frac{\sum_{j=1}^{J}\left[w_{ij}I^{\rm o}_{\mathbf{h}_i}(\mathbf{y}_j) - w_{ij}I^{\rm c}_{\mathbf{h}_i}(\mathbf{y}_j)\right]^2}{\sum_{j=1}^{J}w_{ij}^2(I^{\rm o}_{\mathbf{h}_i})^2(\mathbf{y}_j)}\right\}^{1/2}\theta\left[x, P^{\rm o}_{\mathbf{h}_i}(\mathbf{y}_j)\right] \qquad (8)$$

and

$$\overline{R}_{wx} = (1/I)\sum_{i=1}^{I}R_{wx}(\mathbf{h}_i)$$

or

$$R_{wx} = \left\{\frac{\sum_{i=1}^{I}\sum_{j=1}^{J}\left[w_{ij}I^{\rm o}_{\mathbf{h}_i}(\mathbf{y}_j) - w_{ij}I_{\mathbf{h}_i}(\mathbf{y}_j)\right]^2}{\sum_{i=1}^{I}\sum_{j=1}^{J}w_{ij}^2(I^{\rm o}_{\mathbf{h}_i})^2(\mathbf{y}_j)}\right\}^{1/2}\theta\left[x, P^{\rm o}_{\mathbf{h}_i}(\mathbf{y}_j)\right], \qquad (9)$$

with

$$I_{\mathbf{h}_i}(\mathbf{y}_j) = P_{\mathbf{h}_i}(\mathbf{y}_j)N_{\mathbf{h}} \quad \text{(diffracted intensity)},$$

$$w_{ij} = \left[I_{\mathbf{h}_i}(\mathbf{y}_j)\right]^{-1/2} \quad \text{(diffracted intensity weight)}.$$

These R factors correspond to the R_{wp} factors of Rietveld analysis.

4. Texture strength factors

Once $f(g)$ is satisfactorily obtained, one can calculate factors that give an estimate of the overall texture strength. Caution should be taken here when comparing samples on the basis of overall texture strength parameters. Samples should have the same crystal symmetry and exhibit similar texture components. However, such factors are indicated to see the possible evolution of the reliability factors, which are themselves overall parameters, with the texture strength.

Two texture strength estimators are used here. Firstly, the texture index (Bunge, 1982), expressed in m.r.d.^{2}, is the normalized sum of squared density values,

$$F^2 = (1/8\pi^2)\sum_i\left[f(g_i)\right]^2\Delta g_i, \qquad (10)$$

where $\Delta g_i = \sin\vartheta_i\Delta\vartheta\,\Delta\varphi\,\Delta\gamma$ is the ODF cell volume.

The second overall texture strength parameter is a measure of the texture disorder, evaluated by the calculation of the entropy:

$$S = (1/8\pi^2)\sum_i f(g_i)\ln f(g_i)\Delta g_i. \qquad (11)$$

5. Results and discussion

5.1. Real-sample orientation distributions

The results presented here come from numerous ODF refinements, on nearly 150 samples, including various crystal symmetry and phases: PST, MgO and PZT (Chateigner, Wenk, Patel *et al.*, 1997; Chateigner, Lutterotti & Hansen, 1997; Chateigner, Wenk & Pernet, 1997), PTL (Ricote *et al.*, 1999; Ricote & Chateigner, 1999), PTC (Ricote *et al.*, 2000, 2002), Ag (Wenk, Chateigner, Pernet, Bingert *et al.*, 1996), nontronite (Manceau *et al.*, 1998), Pt (Chateigner, Wenk, Patel *et al.*, 1997; Chateigner, Lutterotti & Hansen, 1997; Chateigner, Wenk & Pernet, 1997; Ricote & Chateigner, 1999; Ricote *et al.*, 2000), $YBa_2Cu_3O_7$ and Y_2BaCuO_5 (Chateigner, Wenk & Pernet, 1997; Chateigner, Ricote *et al.*, 1999; Chateigner, Hedegaard & Wenk, 1999; Chateigner, Wenk & Pernet, 1999), $Bi_4(V,Co)_2O_{11}$ (Muller *et al.*, 1996), HgI_2 (Chateigner & Erler, 1997), $Bi_2Sr_2Ca_2Cu_3O_{10}$ (Wenk, Chateigner, Pernet & Ouladdiaf, 1996), $Bi_2Sr_2Ca_1Cu_2O_8$ (Wenk, Chateigner, Pernet, Bingert *et al.*, 1996; Pavard *et al.*, 2000), aragonite (Chateigner, Hedegaard & Wenk, 1999; Chateigner *et al.*, 2000), calcite (Hacker *et al.*, 2000; Chateigner, Morales & Harper, 2002), quartz (Chateigner, Wenk & Pernet, 1999; Hacker *et al.*, 2000; Ratschbacher *et al.*, 2000; Chateigner, Camana & Trimby, 2002; Camana *et al.*, 2002), biotite and albite (Chateigner, Wenk & Pernet, 1999), Si_3N_4 and SiC (Chateigner, Lutterotti & Hansen, 1997), $Nd_2Fe_{14}B$ (Rivoirard *et al.*, 2000), Bi_3TiNbO_9 (Ricote *et al.*, 2001), $(SrBi_2Nb_2O_9)_{1-x}(Bi_3TiNbO_9)_x$ ceramics (Moure *et al.*, 2002), amphiboles, eclogites and glaucophane (Zucali *et al.*, 2002), $LiNbO_3$ (Bornand *et al.*, 2002), $ErMn_4Fe_8C$ (Morales *et al.*, 2003), polypropylene (Aouinti *et al.*, 2002), $(La,Li)TiO_3$ (Morales *et al.*, 2002), and Ni-modified silicates (Richard-Plouet *et al.*, 2003). These experiments have been performed using various instruments, radiation, wavelengths and detectors, and variable numbers of pole figures have been taken into account in the refinements.

Fig. 1 shows how the RP_0 and RP_1 factors vary with the texture strength. Dispersion of the points is observed, since the reliability factors depend on the quality of the measurements. In this study, since the ODF is calculated on the basis of discrete measurements using $5 \times 5^\circ$ grids, one cannot expect to determine quantitatively textures for which the FWHM of the dispersion is smaller than 5° at minimum. The *BEARTEX* texture package recommends, in fact, 7.5° when using the WIMV algorithm. We took this limit in Fig. 1(*a*), which corresponds to a texture index of around 300 m.r.d.^{2} on average. It can be seen that both RP_0 and RP_1 factors evolve with the texture strength in a similar manner. This variation conserves the same global shape at small texture strengths (Fig. 1 *b*) and apparently does not depend on the crystal structure at the resolution of our experiments.

Fig. 1(*c*) shows the relationship between RP_1 and RP_0 values. Such a curve shows the stability or homogeneity of the factors for the representation of different texture levels. The RP_1 values are in general smaller than the RP_0 values, which is a possible indication that the algorithm tends to favour the reproduction of high-density values. However, this is not the case, as we will see later, but is only the signature of the *RP* factor dependency. Indeed, since the RP_0 values are calculated for all density levels, they also include RP_1 data and their value is consequently larger. Furthermore, the other *R* factors do not show the same behaviour. Therefore, RP_0 gives more importance to the differences in low density levels than RP_1 does for the levels above 1 m.r.d. This behaviour disappears for the weighted factors RP_w and R_w. An equivalent repre-

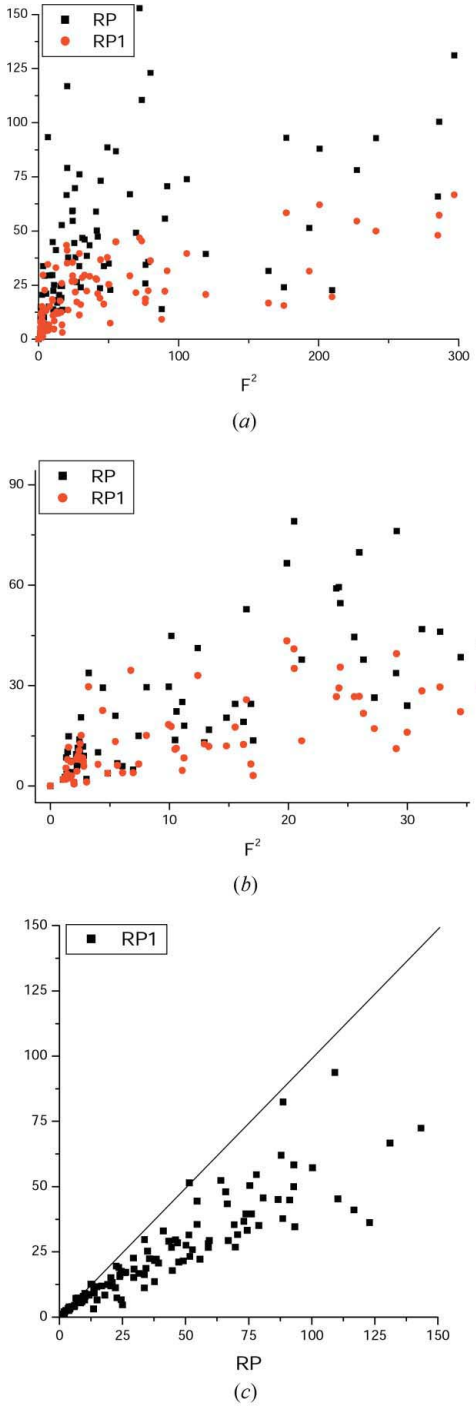

Figure 1
Variation of the experimental *RP* factors RP_0 (*a*) and RP_1 (*b*) with F^2, for two different ranges of F^2, and their correlation (*c*). The straight line corresponds to $RP_0 = RP_1$.

sentation of large and small density levels would correspond on this figure to a one-to-one equal-representation straight line as indicated, which is clearly not the case for *RP* factors. For strong textures, the point dispersion increases similarly for both factors, which is another sign of the strong *RP* variation with texture strength.

The surface-weighted RP_w factors (Fig. 2) exhibit, as expected, less dependency on texture strength. This fact proves the efficiency of the weighting process, particularly for the higher texture strengths. The correlation between RP_{w1} and RP_{w0} consequently appears as an almost perfect line, showing that the lack of weight in the *RP* factors explains the variations from one-to-one correlation of Fig. 1(*c*), rather than a WIMV algorithm effect. However, there is still some deviation from a perfect linear correlation, which indicates a possible improvement in density level representation. Experiments that deviate from the straight line have probably favoured one or the other density range during the refinement and may have to be revisited.

Data for the weighted factors R_w are presented in Fig. 3. These factors exhibit the lowest dependency with texture strength, and would therefore be indicated for comparing sample ODF refinements. The correlation between R_{w1} and R_{w0} is also less dispersed than that for *RP* factors, but roughly comparable to that of RP_w factors. However, the dispersion of the correlation is more homogeneous with the texture strength in the case of R_w factors than for other *R* factors.

As a matter of fact, all *R* factors depend on the texture strength, but some to a lesser degree. The weighting schemes seem to provide similar results from the point of view of comparison of samples, with a tendency of R_w factors to exhibit the smallest dependence with texture strength. If it exists, the *RP* dependence on crystal symmetry is masked by the point dispersion due to ODF refinement imperfections, and does not affect the one-to-one correlation of other factors.

This reliability analysis may also provide some criteria to test the goodness of the ODF refinement. For a given texture analysis, we can appreciate whether the refinement has been

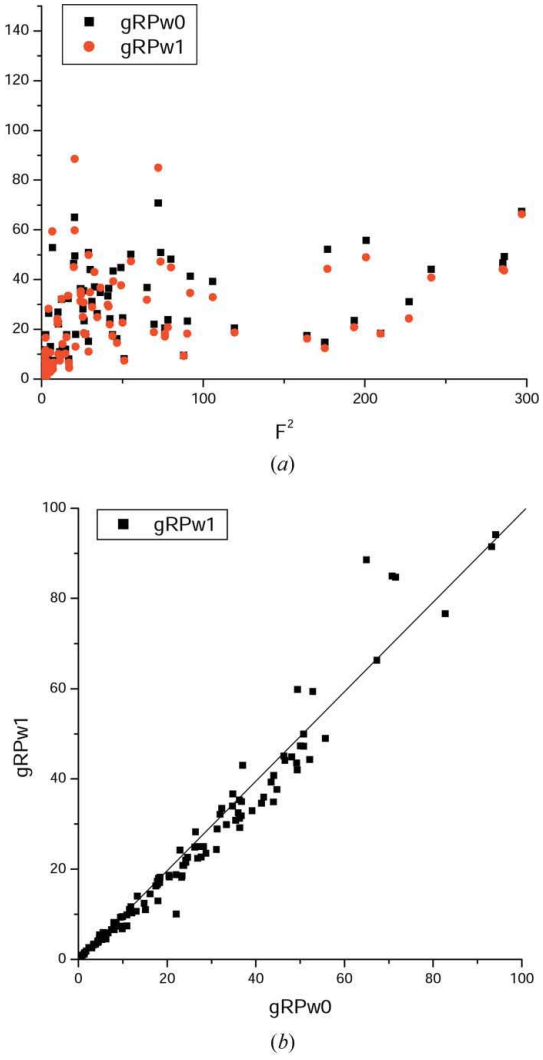

Figure 2
Variation of the surface-weighted *RP* factors RP_{w0} and RP_{w1} (*a*) with F^2, and their correlation (*b*). The straight line corresponds to $RP_{w0} = RP_{w1}$.

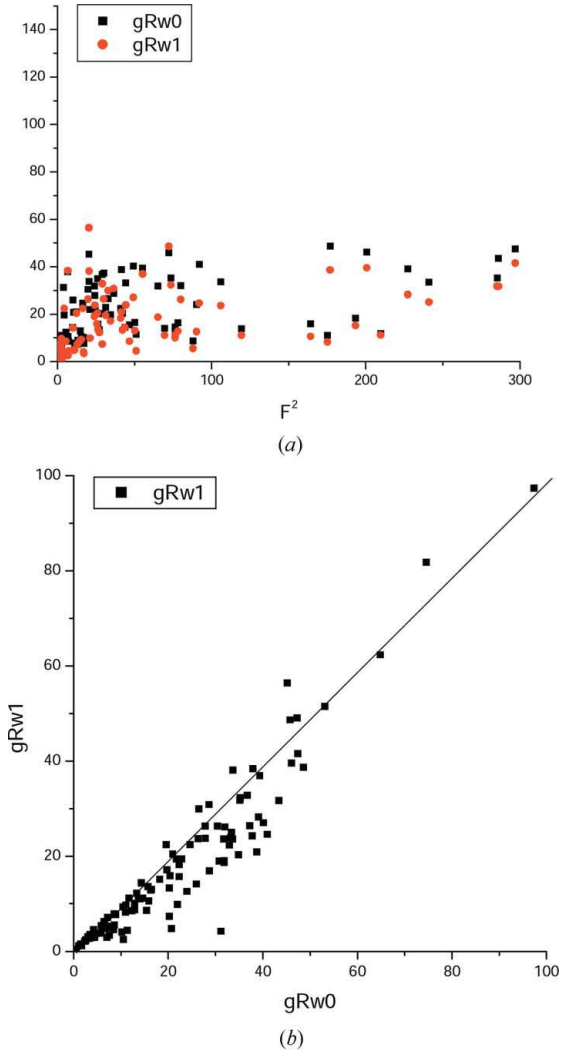

Figure 3
Variation of the weighted R_w factors R_{w0} and R_{w1} (*a*) with F^2, and their correlation (*b*). The straight line corresponds to $R_{w0} = R_{w1}$.

Table 1
Parameters resulting from the refinement of the ODF of modelled texture components with variable FWHMs.

Cyc: number of cycles for stopping the refinement; Exp: exponent parameter entering the convergence speed; {110} dif: difference in maximum density between observed and recalculated {110} pole figures.

F^2 (m.r.d.^{2})	RP_1 (%)	RP_0 (%)	FWHM (°)	$-S$	Cyc	{110} dif (m.r.d.)	Exp
1	0.27	0.4	90	0	2	0	2
1.1	0.68	1.15	60	0.05	17	0	2
1.92	0.92	1.78	45	0.36	28	0.01	2
4.15	1.64	3.21	35	0.94	36	0.05	2
11.56	3.07	6.38	25	1.92	24	0.08	2
23.21	5.03	6.29	20	2.64	27	0.12	2
56.89	7.43	8.9	15	3.51	17	0.29	0.5
69.48	7.08	9.41	14	3.7	6	0.41	0.5
112.05	7.86	11.09	12	4.18	8	0.7	0.5
199.8	6.82	13.59	10	4.75	16	1.42	0.5
285.05	7.46	15.15	9	5.08	11	3.07	0.5
431.91	11.07	18.21	8	5.44	15	4.63	0.5
704.35	17.75	15.79	7	5.87	12	7.48	0.5
–	22.89	28.39	6.9	6.4	5	14.1	0.5

operated in a subjective manner; in the R correlation curves, if the corresponding point is not placed on the 45° line on the weighted factor plots, the operator has probably focused on some details of the analysis without considering the others. In certain cases this may be reasonable, but has to be justified. For instance, on the R_w graph (Fig. 3), one can observe points that are under the 45° line. These have been obtained on a series of heteroepitaxial films with multiple heteroepitaxial relationships. The operator then concentrated on identifying the major texture components, giving importance to the RP_1 factors during the ODF refinement.

5.2. Modelled distributions

The theoretical limit that one can reach using the WIMV technique and a 5 × 5° scan grid can be checked on modelled ODF components with Gaussian shapes of varying FWHM (Table 1). We chose to use a cubic crystal symmetry with one texture component **g** = (0, 0, 0) (Fig. 4*a*), and to refine the ODF from the model {110} complete pole figure. The refinement process was stopped when a convergence velocity of 0.1 was reached, or when the RP_0 factor was larger than that for the $(n - 1)$ cycle. Fig. 4(*b*) shows the RP evolution of the modelled texture with the texture strength in the 0–300 m.r.d.^{2} range. Since the refinement is performed on noiseless and perfect distributions, the RP values are correspondingly considerably lowered compared with real experiments. However, it is clearly seen that RP values increase with F^2 for modelled components, which means that the WIMV algorithm has some difficulties in reproducing textures when the width of the dispersion becomes close to the experimental resolution related to the scan grid. It would be interesting to compare these results with the sensitivity to experimental resolution of other discrete methods such as ADC. However (Fig. 4*c*), even for low texture strength, for which the distribution width is larger than several times the scan grid, one can see this increase in RP factors. Undoubtedly, this increase is then an intrinsic behaviour of RPs and is not due only to the WIMV refinement strategy. The non-monotonous variation observed for RP_0 and RP_1 factors is due to the choice of the exponent parameter of the WIMV approach (Table 1), which has to be modified, depending also on F^2, in order to fit experimental data better. This parameter may also be fitted, but we chose here to vary it by steps of 0.5 in the 0.5–2.5 range and conserved the results for the lower RP_0.

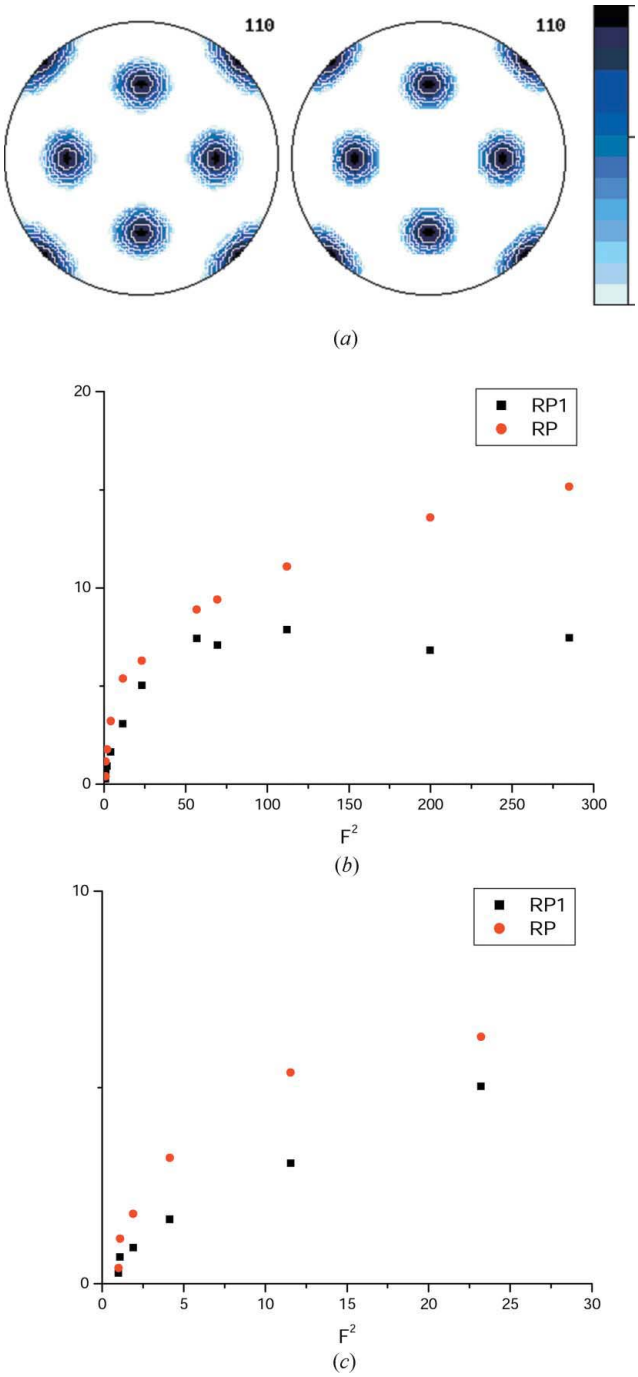

Figure 4
(*a*) Simulated (left) and recalculated (right) {110} pole figure of a cubic crystal system in the **g** = (0, 0, 0) orientation with a 10° FWHM (logarithmic density scale, equal area projection, maximum = 52 m.r.d., minimum = 0). (*b*) Variation of the corresponding RP factors with F^2 up to F^2 = 300 m.r.d.^{2} and (*c*) RP *versus* F^2 in the 0–30 m.r.d.^{2} range.

The sensitivity of the WIMV algorithm to measurement resolution is included in the evolutions of the *RP* values obtained from real experiments, but as one can see in modelled experiments, this contribution cannot alone account for all the variations observed in real experiments. In the latter, the resolution sensitivity of the method is combined with the true experimental reliability, in a non-trivial way, and ideally should be removed. We may imagine calibration processes to correct for the sensitivity of the algorithm, but in the absence of a real physical or statistical fundament.

These simulations help to fix the minimum value of the FWHM, which gives a reliability that is too low in given conditions (ODF refinement method, resolution). For instance, if one accepts a maximum of 10% on the RP_1 values, then an 8.5° dispersion appears as the strongest texture refinable (Fig. 4*b*). This value corresponds to a maximum F^2 of approximately 300 m.r.d.^{2}.

5.3. Correlation between F^2 and S

Entropy and texture index are correlated, but from their definition it would be difficult to obtain an analytical expression for this correlation. Looking at the variation of the entropy with the texture index (Fig. 5*a*), the modelled textures of Table 1 are placed on a single curve in the case of single-component and cubic crystal symmetry ODFs. Conversely, real experiments (Fig. 5*b*) show large deviations of the points from the modelled curve.

Fig. 5 illustrates the relative evolutions of the texture strength parameters, which result from their analytical expressions; below a value of around 50 m.r.d.^{2}, S varies much more than F^2, this latter being less efficient in revealing the texture strength. The reverse is true above 50 m.r.d.^{2}. It is therefore proposed that it is better to use S and F^2 in different ranges of texture strength, typically S below 50 m.r.d.^{2} and F^2 above.

The deviation from the model curve (Fig. 5*b*) is, in principle, not a comparison between experimental and recalculated data, but only the expression of calculation of the ODF. However, real experiments show discrepancies from the model curve, and examination of the points did not reveal any regular dependence with specific ODF components. These variations, as for the *R* factors, may mask any regular dependence of the points on peculiarities of the ODF such as crystal symmetry or components. Interestingly, the model curve is centred on the real experimental one, indicating either that the chosen model corresponds to the averaged variability of the curve or that this is a unique curve that does not depend on textural components. The former hypothesis would point to a particular characteristic of the **g** = {0, 0, 0} orientation type, which would be hard to understand. Conversely, if reliability information is present in this curve, then another test for a good ODF refinement is available using these data, considering that the modelled texture results are the best refinement that one can reach. Consequently, comparing real experiments with modelled textures would help in identifying one refinement that may be ameliorated.

In order to check for the validity of this new ODF refinement criterion, 26 other modelled ODFs were generated and added to Fig. 5 (Fig. 6*a*, circles). For this test, the crystal symmetry, number of texture components (up to four), *g* components (including fibre textures) and component dispersion (from 10 to 30° FWHM) were varied in order to represent orientation distributions up to texture indexes close to 1000 m.r.d.^{2}. Several conclusions can be drawn from this analysis.

(i) All the ODF points are located on the same curve; this is believed to be a unique behaviour of $f(g)$ in the analysis uncertainties, which mainly arise from the resolution of the calculation grid.

(ii) The crystal symmetry only moves the points on this curve, lower symmetries being located at larger F^2 values.

(iii) As expected, lower component dispersions are located at larger F^2 values, whereas a larger number of components decreases F^2.

(iv) Neither the number of pole figures taken into account in the refinement nor the pole figures themselves affect the position of the point on the curve, provided that enough information is given to the ODF refinement.

In Fig. 6(*a*), the crossed point corresponds to a refinement on a modelled ODF for which the refinement has been

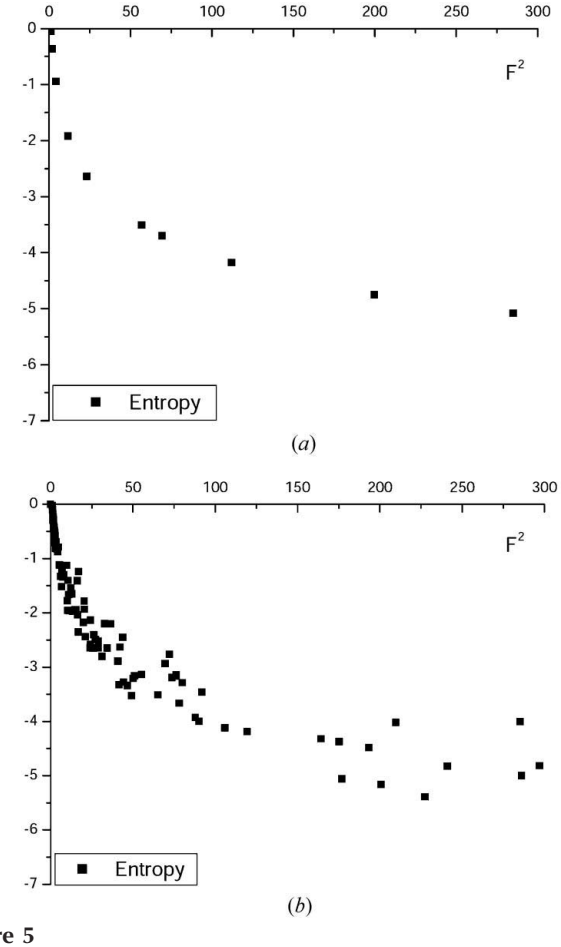

Figure 5
Entropy-to-texture index relationship. (*a*) Modelled textures with the **g** = {0, 0, 0} component of texture; (*b*) real samples.

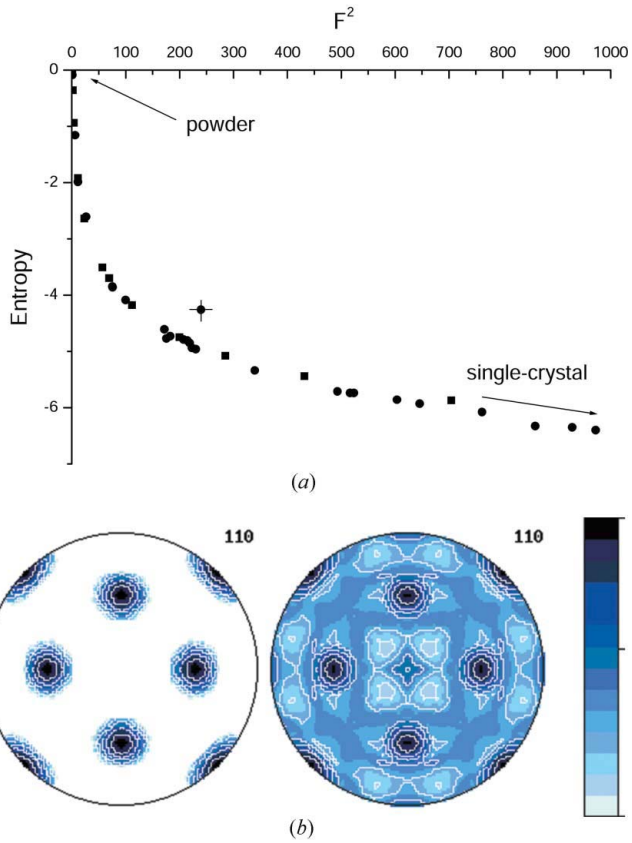

Figure 6
(*a*) Entropy-to-texture index relationship of modelled textures. Squares are the same points as in Fig. 5(*a*); circles are computed for various texture components and crystal symmetries. (*b*) Simulated (left) and recalculated (right) {110} pole figure of a cubic crystal system in the **g** = (0, 0, 0) orientation with a 9° FWHM (logarithmic density scale, equal area projection, maximum = 37 m.r.d., minimum = 0).

stopped before it reached the minimum value. This is therefore a bad refinement, and the recalculated pole figures do not compare favourably with the experimental ones (Fig. 6*b*). This point is not on the $S(F^2)$ curve, and the distributions observed in Fig. 5(*b*) are then explained by discrepancies (lower reliabilities) in the ODF refinements. Since the ODF refinement reliability decreases at larger texture strengths, for a given resolution, the deviations from the modelled curve are consequently larger for large F^2 values.

6. Conclusions

Reliability factor uses in quantitative texture analysis have been tested experimentally for texture strengths, on real and modelled distributions. The classical *RP* factors exhibit the strongest variations with texture strengths, as revealed by their dependency on the texture index. Weighted factors are less dependent on this strength, with the lowest variability for R_w factors. The stability of the ODF refinement reliability represented by *R* factors is best characterized by $R_1(R_0)$ plots, which show that the R_w factors exhibit the most regular stability among density levels. The entropy *versus* texture index relationship demonstrates experimentally that all ODFs are represented by a single $S(F^2)$ curve, from which the ODF refinement reliability can also be tested. Two ranges of this curve can be separated in the view to compare the texture strengths of samples. For lower texture strengths (typically below 50 m.r.d.^{2}) the entropy exhibits a larger variability than F^2 and should be used to compare samples, whereas the reverse applies for strengths larger than around 50 m.r.d.^{2}.

This work could not have been carried out without support from the following institutions, through constant financial awards or contracts: Ministère de l'Enseignement Supérieur et de la Recherche, Délégation Régionale à la Recherche et à la Technologie, Basse-Normandie, CNRS–CSIC French–Spanish cooperation 'Crystallographic texture influence on polycrystalline ferroelectric materials properties' (contract No. 2004FR0030) and 'PTL, SBT and PTC ferroelectric film characterization' (contract No. 8540, 2000–2001), European project ESQUI 'X-ray expert system for microelectronic films quality improvements', and European Concerted Action 'Application of ferroelectric thin films for SAW devices' (COST No. 514, 1998).

References

Aouinti, M., Chateigner, D., Gibaud, A. & Poncin-Epaillard, F. (2002). *Mater. Sci. Forum*, **408–412**, 1579–1584.
Bornand, V., Huet, I., Bardeau, J.-F., Chateigner, D. & Papet, Ph. (2002). *Integr. Ferroelectr.* **43**, 51–64.
Bunge, H.-J. (1982). *Texture Analysis in Materials Science*, translated by P. R. Morris. London: Butterworths.
Bunge, H.-J. & Esling, C. (1982). Editors. *Quantitative Texture Analysis*. Oberursel: DGM.
Camana, G., Chateigner, D., Zucali, M. & Artioli, G. (2002). *Am. Mineral.* **87**, 1128–1138.
Chateigner, D. (2002). CNRS-INEL Licence No. L03048.
Chateigner, D., Camana, G. & Trimby, P. (2002). *Mater. Sci. Forum*, **408–412**, 1675–1680.
Chateigner, D. & Erler, B. (1997). *Mater. Sci. Eng.* **45**, 152–161.
Chateigner, D., Hedegaard, C. & Wenk, H.-R. (1999). *Texture of Materials*, Vol. 1, edited by J. A. Szpunar, pp. 1327–1332. Ottawa: NRC Research Press.
Chateigner, D., Hedegaard, C. & Wenk, H.-R. (2000). *J. Struct. Geol.* **22**, 1723–1735.
Chateigner, D., Lutterotti, L. & Hansen, T. (1997). *ILL Highlights*, **1997**, 28–29.
Chateigner, D., Morales, M. & Harper, E. M. (2002). *Mater. Sci. Forum*, **408–412**, 1687–1692.
Chateigner, D., Ricote, J., Chaud, X., Gautier-Picard, P., Beaugnon, E., Soubeyroux, J.-L., Leblond, C. & Monot, I. (1999). *Textures of Materials*, Vol. 1, edited by J. A. Szpunar, pp. 457–462. Ottawa: NRC Research Press.
Chateigner, D., Wenk, H.-R., Patel, A., Todd, M. & Barber, D. J. (1997). *Integr. Ferroelectr.* **19**, 121–140.
Chateigner, D., Wenk, H.-R. & Pernet, M. (1997). *J. Appl. Cryst.* **30**, 43–48.
Chateigner, D., Wenk, H.-R. & Pernet, M. (1999). *Textures Microstruct.* **33**, 35–43.
Hacker, B. R., Ratschbacher, L., Webb, L. E., McWilliams, M., Calvert, A., Dong, S., Chateigner, D. & Wenk, H.-R. (2000). *J. Geophys. Res.* **105**, 13339–13364.
Hamilton, W. C. (1965). *Acta Cryst.* **18**, 502.

Hill, R. J. & Fisher, R. X. (1990). *J. Appl. Cryst.* **23**, 462.
Kocks, U. F., Tomé, C. N. & Wenk, H.-R. (1998). *Texture Anisotropy*, p. 676. Cambridge University Press.
Manceau, A., Chateigner, D. & Gates, W. P. (1998). *Phys. Chem. Miner.* **25**, 347–365.
Matthies, S. & Vinel, G. W. (1982). *Phys. Status Solidi B*, **112**, K111–K114.
Matthies, S., Vinel, G. W. & Helming, K. (1987). *Standard Distributions in Texture Analysis*, edited by S. Matthies. Berlin: Akademie Verlag.
Morales, M., Chateigner, D. & Fruchart, D. (2003). *J. Magn. Magn. Mater.* **257**, 258–269.
Morales, M., Laffez, P., Chateigner, D. & Vickridge, I. (2002). *Thin Solid Films*, **418**, 119–128.
Moure, A., Ricote, J., Chateigner, D., Millan, P., Castro, A. & Pardo, L. (2002). *Ferroelectrics*, **270**, 9–14.
Muller, C., Chateigner, D., Anne, M., de Rango, P., Fouletier, J. & Bacmann, M. (1996). *J. Phys. D*, **29**, 3106–3112.
Pavard, S., Bourgault, D., Villard, C., Tournier, R., Rivoirard, S. & Chateigner, D. (2000). *Inst. Phys. Conf. Ser.* **167**, 207–210.
Pawlik, K. (1993). *Mater. Sci. Forum*, **133–136**, 151–156.
Ratschbacher, L., Hacker, B. R., Webb, L. E., Calvert, A., Ireland, T. R., McWilliams, M. O., Dong, S., Chateigner, D. & Wenk, H.-R. (2000). *J. Geophys. Res.* **105**, 13303–13338.
Richard-Plouet, M., Guillot, M., Chateigner, D., Traverse, A. & Vilminot, S. (2003). *Nucl. Instrum. Methods Phys. Res. Sect. B*, **200**, 148–154.
Ricote, J. & Chateigner, D. (1999). *Bol. Soc. Esp. Cerám. Vidrio*, **38**, 587–591.
Ricote, J., Chateigner, D., Calzada, M. L. & Mendiola, J. (2002). *Bol. Soc. Esp. Cerám. Vidrio*, **41**, 80–84.
Ricote, J., Chateigner, D., Pardo, L., Algueró, M., Mendiola, J. & Calzada, M. L. (2000). *Ferroelectrics*, **241**, 167–174.
Ricote, J., Chateigner, D., Ripault, G., Pardo, L., Alguero, M., Mendiola, J. & Calzada, M. L. (1999). *Textures of Materials*, Vol. 2, edited by J. A. Szpunar, pp. 1327–1332. Ottawa: NRC Research Press.
Ricote, J., Pardo, L., Moure, A., Castro, A., Millán, P. & Chateigner, D. (2001). *J. Eur. Ceram. Soc.* **21**, 1403–1407.
Rietveld, H. M. (1969). *J. Appl. Cryst.* **2**, 65–71.
Rivoirard, S., Chateigner, D., de Rango, P., Fruchart, D., Perrier de la Bathie, R. & Soubeyroux, J.-L. (2000). *Philos. Mag. A*, **80**, 1955–1966.
Rothstein, S. M., Richardson, M. F. & Bell, W. D. (1978). *Acta Cryst.* A**34**, 969–974.
Ruer, D. & Baro, R. (1977). *Adv. X-ray Anal.* **20**, 187.
Toraya, H. (1986). *J. Appl. Cryst.* **19**, 440–447.
Wenk, H. R. (1985). Editor. *Preferred Orientation in Deformed Metals and Rocks: An Introduction to Modern Texture Analysis*. London: Academic Press.
Wenk, H.-R., Chateigner, D., Pernet, M., Bingert, J., Hellstrom, E. & Ouladdiaf, B. (1996). *Physica C*, **272**, 1–12.
Wenk, H.-R., Chateigner, D., Pernet, M. & Ouladdiaf, B. (1996). *Texture of Materials*, Vol. 2, edited by Z. Liang, L. Zuo & Y. Chu, pp. 1070–1075. London: Academic Publishers.
Wenk, H.-R., Matthies, S., Donovan, J. & Chateigner, D. (1998). *J. Appl. Cryst.* **31**, 262–269.
Wenk, H.-R., Pawlik, K., Pospiech, J. & Kallend, J. S. (1994). *Texture Microstruct.* **22**, 233–260.
Young, R. A., Prince, E. & Sparks R. A. (1982). *J. Appl. Cryst.* **15**, 357–359.
Zucali, M., Chateigner, D., Dugnani, M., Lutterotti, L. & Ouladdiaf, B. (2002). *Deformation Mechanisms, Rheology and Tectonics: Current Status and Future Perspectives*, Vol. 200, edited by S. de Meer, M. R. Drury, J. H. P. de Bresser & G. M. Pennock, pp. 239–253. London: Geological Society Special Publications.